Oscillatory brain activity associated with skin conductance responses in the context of risk

Patrick Ring,[1]* Julian Keil,[2]* Muthuraman Muthuraman,[3] Stephan Wolff,[4] Til Ole Bergmann,[5,6,7] Catharina Probst,[8] Levent Neyse,[9,10,11] Ulrich Schmidt,[1,12,13] Thilo van Eimeren,[14,15] and Christian Kaernbach[2]

[1]*Kiel Institute for the World Economy, Kiel, Germany;* [2]*Department of Psychology, Kiel University, Kiel, Germany;* [3]*Movement Disorders and Neurostimulation, Biomedical Statistics and Multimodal Signal Processing Unit, Department of Neurology, University Medical Center of the Johannes Gutenberg University Mainz, Mainz, Germany;* [4]*Department of Radiology and Neuroradiology, Kiel University, Kiel, Germany;* [5]*Neuroimaging Center, Focus Program Translational Neuroscience, Johannes Gutenberg University Medical Center, Mainz, Germany;* [6]*Leibniz Institute for Resilience Research, Mainz, Germany;* [7]*Department of Neurology and Stroke, Hertie Institute for Clinical Brain Research, University of Tübingen, Tübingen, Germany;* [8]*Department of Neurology, Kiel University, Kiel, Germany;* [9]*German Institute for Economic Research, Research Infrastructure Socio-Economic Panel (SOEP), Berlin, Germany;* [10]*Berlin Social Science Center, Berlin, Germany;* [11]*Institute of Labor Economics, Bonn, Germany;* [12]*Department of Economics and Econometrics, University of Johannesburg, Johannesburg, South Africa;* [13]*Department of Economics, Kiel University, Kiel, Germany;* [14]*Department of Nuclear Medicine, University of Cologne, Cologne, Germany; and* [15]*Department of Neurology, University of Cologne, Cologne, Germany*

INTRODUCTION

Peripheral responses, such as changes in skin conductance (SC), reflect emotional states and are correlated with aspects of behavior. For example, in the Iowa Gambling Task (IGT), healthy control participants produce skin conductance responses (SCRs) preceding disadvantageous decisions (1). Related, but in very different fields of behavior, it has been observed that false somatic feedback can alter individual judgments: listening to dummy heart beats, for example, changes both attractiveness ratings of erotic images (2) and ethical behavior (3). Peripheral responses have broadly proven

* P. Ring and J. Keil contributed equally to this work.
Correspondence: P. Ring (patrick.ring@ifw-kiel.de).

to be useful indicators of various cognitive and emotional processes including threat conditioning, attention, and cognitive effort (4, 5). Considering the correlative nature of this relationship, it appears relevant to identify the central nervous basis of peripheral responses, that is, the cortical correlates of their generation and reafferent representation. Understanding the cortical correlates of peripheral responses can provide insights into their connection to behavior and to emotional and cognitive processes (6). In this study, we focus on SCRs in the context of risk.

Insights into the central nervous basis of SCRs have been gained from studies involving patients with brain lesions (7–9), direct electrical stimulation of specific brain regions (10, 11), and functional imaging studies (12–16). In a nutshell, these studies suggest that several neural pathways appear capable of producing SCRs and the related brain activity depends on the type of stimulus and on the SCR function (for more detailed information please see, Refs. 4 and 5). Patients with brain lesions of the amygdala or ventromedial prefrontal cortex (VMPFC), for example, fail to produce anticipatory SCRs in the IGT (i.e., to motivationally relevant stimuli) but not to noise bursts (i.e., to physical stimuli) (9). Moreover, patients with VMPFC lesions generate SCRs at the outcome phase of the IGT (i.e., when rewards or losses are revealed and processed) but not preceding the card selection (i.e., at the moment where SCRs potentially indicate disadvantageous decisions) (1).

Studying fluctuations of electrical cortical activity using electroencephalography (EEG) or magnetencephalography (MEG) provide insights into the central nervous basis of cognition and behavior (17). Neural oscillations, the fluctuations of cortical excitability of neuron populations, are present all over the cortex and are relevant to most, if not all, cortical functions. They bias input selection, influence sensory processing, and support information transfer between cortical areas (18). Importantly, specific frequencies of neural oscillations have been implicated in decision making (e.g., β-band, 12–24 Hz; 19), attention and stimulus selection (e.g., α-band, 8–12 Hz; 20), and reflect arousal (e.g., α- and β-band; 21 and 22). With respect to risk perception, an EEG study found a reduction of α-band power before feedback in social high-risk decisions (23). However, little is known about the spectral fingerprints of the cortical correlates of risk-sensitive SCRs.

The present study aims at contributing to our understanding of the cortical correlates of risk-sensitive SCRs. Risk sensitive in our context refers to SCRs that were generated after processing information about the occurrence of a future aversive event. In contrast to previous studies, we applied methods with a high temporal resolution to account for the original properties of underlying sympathetic activity, that is, a stable zero baseline with fast single bursts of increased activity (24, 25). Continuous decomposition analysis of electrodermal activity results in precise information about the temporal position of these bursts (26), which in our study served as event markers for the subsequent analyses of electrical cortical activity from EEG data. We did not study the form of the SCR but used temporal information about the SCR peak to assess neural oscillations related to this activity. Electrodermal activity and high-density EEG data were simultaneously recorded during the anticipation of unpleasant but not painful electric shocks with a varying probability of occurrence in a card game. Previous research suggests that SCRs during the anticipation of electric shocks are asynchronously distributed during the anticipation phase (27). Thus, brain activity related to SCRs in such a design should not be systematically related to stimulus processing.

METHODS

Participants

Twenty-five right-handed male undergraduate psychology students (age: M = 23.7 yr, SD = 4.8) took part in the current study as part of their educational program. All participants gave written informed consent and could decide to discontinue participation at any time. The local Ethics Committee of the University Hospital in Kiel, Germany, approved the research design, and the study was performed in agreement with the 2008 Declaration of Helsinki. Six participants had to be excluded due to too few detected SCR peaks, reducing the final sample to 19 participants (age: M = 23.7 yr, SD = 5.2).

Experimental Procedure

The threat-of-shock task, which is inspired by Preuschoff et al. (28) and has been used in previous studies (27, 29), had two stages (Fig. 1). In the first stage, the probability of receiving an electric shock was revealed. In the second stage, the electric shock was either applied or not depending on the previously announced probability. The information about the shock probability in the first stage was coded as a combination of a bet type (higher or lower) and a card value (1 to 10). The bet type was displayed during card selection as an arrow in the middle of the screen (↑ = higher card wins, ↓ = lower card wins) and alternated in each round. The card value was revealed after the participant had drawn 1 out of 10 facedown cards using computer keys with the dominant hand. This was followed by the anticipation phase that was indicated by lighter colors of the face-down cards. After an anticipation phase of ∼8 s, the computer drew 1 out of the remaining 9 cards. If the participant had lost the bet, an electric shock was applied in 50% of the cases. First, based on the card values and second, based on the 50% shock probability, there were 10 different combined electric shock probabilities (in percent, rounded to the next integer): 0, 6, 11, 17, 22, 28, 33, 39, 44, and 50. Because participants were informed that the card values in the initial deck ranged from 1 to 10 and each value existed only once, the first stage revealed the probability of receiving an electric shock. At the end of each round, participants were asked to answer a control question to control for attention. Wrong answers or failing to respond within a 1.5-s time interval led to an electric shock. In 98% of the cases, participants answered the control questions correctly. We, therefore, included all trials in the subsequent analysis. In Fig. 1, the experimental design is graphically illustrated. In this example, the higher card won, which was indicated by an upward arrow during the card selection. The participant drew a card value of 3, indicating a 78% probability of the computer drawing a higher card, that is, a shock probability of 39% (78% × 50%). Here, the computer-drawn card had a value of 9. Because the computer had the higher card value, the participant lost this round and—with a 50%
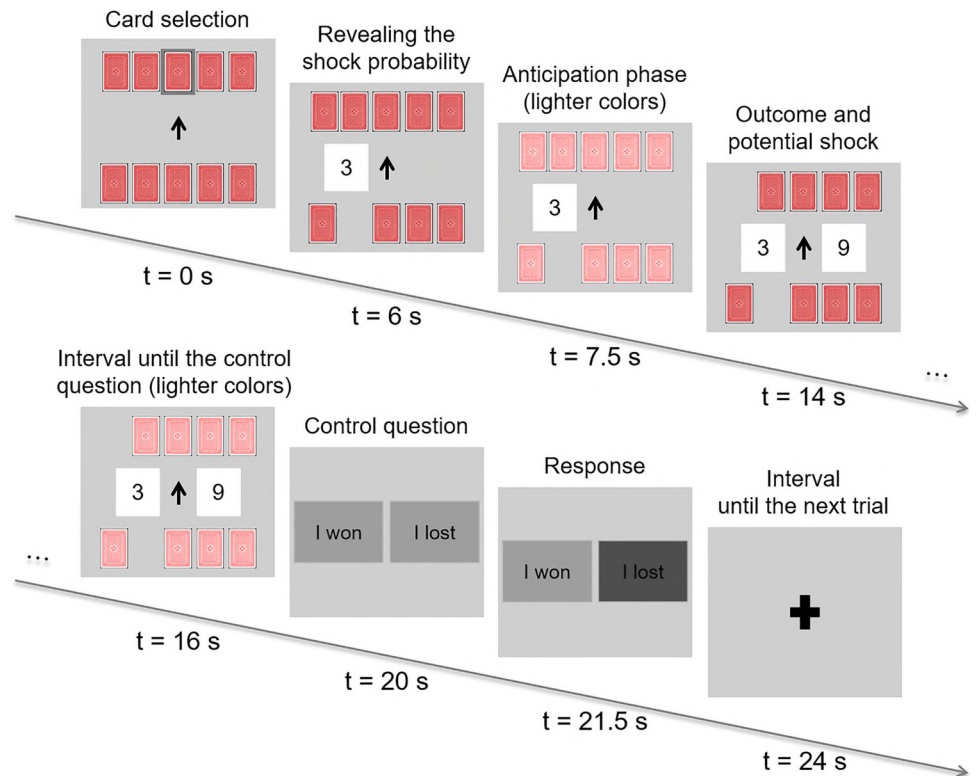
Figure 1. Experimental design. Participants chose 1 out of 10 cards. The card value together with information about the bet type (↑ = higher card wins, ↓ = lower card wins) indicated the probability of receiving an electric shock after an anticipation phase of ~8 s. Electric shock was applied when the second card was revealed. Subsequently, participants were asked to answer a control question.

probability—received an electric shock when the second card was revealed. In previous studies, it was reported that this experimental design resulted in risk-sensitive SCRs during the anticipation phase, that is, SCRs that correlated positively and significantly with the shock probability (27, 29, 30).

Participants played two blocks with 30 rounds each. The card values were arranged such that each shock probability occurred three times within a block. The software package Psychtoolbox-3 (www.psychtoolbox.org) running on MATLAB 2012b (MathWorks Inc.) was used for stimulus presentation and response acquisition.

Electric Shock Stimulation

Electric shocks were given via two Ag-AgCl electrodes (10 mm diameter) attached to the medial phalanges of digits II and III of the dominant hand. The electrodes were connected via BNC cables to the electrostimulator (Rehastim, HasoMed GmbH, current = 0–126 mA, pulse width = 500 μs, frequency = 100 Hz). Shock levels increased linearly in milliampere and number of single bursts, that is, level 1 = 1 burst with 1 mA, level 2 = 2 bursts with 2 mA, etc. As the time interval between the single bursts was very small (100 μs), participants perceived them as a single event. Participants were told that we were looking for an intensity of shock that was unpleasant but not painful. We started with level 1 (usually not yet perceived by the participant) and then increased the level until the participant indicated that this was a painful experience. Then, the previous level was used during the experiment. As participants potentially got used to the level of shock intensity, the shock intensity was calibrated again for the second block of the card game.

SC Measurements

We used a 10-channel bioamplifier (Nexus 10; Mind Media B.V.) and the corresponding recording software BioTrace (Mind Media B.V.) to record electrodermal activity. Following a standard protocol (4), two flat Ag-AgCl electrodes (10 mm diameter) were placed at the medial phalanges of digit II and III of the nondominant hand, and the electrode sites were prepared with an isotonic paste (TD-246, Discount Disposables). As generally recommended by Boucsein (4), there was a 5-min pause between attaching the electrodes and starting the recording. SC data were sampled at 32 Hz.

Analysis of SC Data

SC data were analyzed using the software package Ledalab (V3.4.8), applying continuous decomposition analysis to disentangle phasic components from tonic activity (26). This procedure aims at providing a continuous and temporally precise indicator of sympathetic activity that reflects the original properties of the underlying sudomotor nerve activity, that is, a stable zero baseline with single bursts of increased activity. This so-called phasic driver has the same unit as the original raw data (microsiemens, μS). The time of interest is the anticipation phase (i.e., the phase before the computer's card draw) of the above-outlined card game (see *Experimental Procedure*). SCR peaks with minimum amplitude of 0.05 μS were identified as events (4). Because we were interested in brain activity before and after SCR peaks, we had to make sure that brain activity was risk sensitive, that is, related to the electric shock probability, and at the same time not contaminated by the electric shock

application itself. Therefore, in a first analysis, we only considered SCR peaks that occurred more than 1.5 s after revealing the first card value and more than 1.5 s before revealing the second card value. The identified SCR peaks provided event markers for the subsequent event-related analyses. Due to this approach, it was possible that more than one peak from the same trial was selected for the further analysis. Figure 2 shows a graphical representation of our approach exemplary for one participant.

To verify that our experimental task was successful in electing risk-sensitive SCRs, we tested whether the shock probability had an impact on various SCR measures (integrated SCR, sum of SCR amplitude, and number of SCR peaks). To account for the dependencies among repeated data, we used random intercept models (package lme4 in R), which allow each participant to have a unique intercept (32).

EEG Measurements

EEG data were recorded using a potassium chloride saline solution soaked 256-channel geodesic sensor net (EGI GES 300 system, EGI, Eugene, OR) at a sampling rate of 1,000 Hz, with 0.1 to 250 Hz online bandpass filters and vertex reference. EEG preprocessing and analysis was performed using the open-source MATLAB-toolboxes FieldTrip (33), EEGLab (34), and customized functions for single-trial source projection (available at https://github.com/juliankeil/VirtualTools/).

Analysis of EEG Data

Analysis of EEG data was performed on SCR peaks during the anticipation phase in the above-outlined card game (see *Experimental Procedures*). These brain processes are not only related to SCRs but also reflect general activity due to shock anticipation. To differentiate brain processes related to SCRs and general activity, we applied the following method: for each participant, we generated two sets of SCR peaks. *Set 1* contained real SCR peaks, which were identified based on the above-outlined method (see *Analysis of SC Data*). *Set 2* contained dummy SCR peaks. Dummy SCR

peaks of a certain shock probability were generated by taking the real SCR peaks from all other participants for the same shock probability and applying their latency to the current participant. To control for habituation, we did so only for trials of the same sequential trial position. Moreover, to avoid oversampling of identical data segments later on, we excluded dummy SCR peaks ±1 s around real peaks and ±0.5 s around other dummy peaks. Thus, dummy SCR peaks have identical distributional characteristics as real SCRs, but they are not related to real SCR peaks of the current participant (see Supplemental Fig. S1; all Supplemental material is available at https://doi.org/10.17605/OSF.IO/BWSE4). Brain activity related to dummy SCRs should capture the general activity due to shock anticipation, whereas the difference in brain activity between real and dummy SCRs should capture brain activity specifically related to SCR peaks. Due to this procedure, any differences in EEG data between real and dummy SCR peaks reveal only information about the occurrence of a risk-sensitive SCR peak and nothing about the level of threat anticipation per se, because the level of threat anticipation was perfectly balanced between the two sets of events. The two sets of SCR peaks provided the event markers for the subsequent analyses.

The EEG analysis pipeline consisted of three steps (Supplemental Fig. S2). The first step intended to remove well-known sources of artifacts in EEG data, such as low-frequency drifts, high-frequency muscular artifacts, eye-movement artifacts, and line-noise. First, voltage offsets were removed by subtracting the mean from that data. Data subsequently were filtered using two-pass Hamming-windowed FIR filters, with an order of 3301, a −6-dB cutoff frequency of 0.5 Hz, and a passband edge of 1 Hz for the high pass; an order of 133, a −6-dB cutoff frequency of 112.5 Hz, and a passband edge of 100 Hz for the low pass; and an order of 3301, −6-dB cutoff frequencies of 49.5 and 50.5 Hz, and a stop band from 49 to 51 Hz for the notch filter (35). Next, bad channels were interpolated, data were rereferenced to the common average using robust rereferencing implemented in the PREP toolbox (function "performReference.m"; 36), and the sampling rate was reduced to 250 Hz. After initial processing of the whole data set, 3-s segments around real SCR peaks (means ± SD: 60 ± 20.76 segments) and dummy SCR peaks (171 ± 25.76) were extracted. Segments that exceeded a threshold of ±150 μV were rejected automatically. Independent component analysis using an extended infomax algorithm (37) was performed on the truncated data and components that represented artifacts were removed automatically as implemented in the SASICA toolbox (38). To ensure proper functioning, automatic component removal was manually screened. To ensure similar signal-to-noise ratios, we equalized segment numbers between peak and dummy segments by randomly sampling the lower number of segments from the larger set, and only participants with at least 20 segments for the two conditions were retained (see *Participants*; segments: mean = 49, SD = 19.11; see Supplemental Table S1).

The second step involved the source projection of the signal of interest related to real and dummy SCR peaks and focused on low-frequency oscillations (2–35 Hz). The reason behind this choice was that higher frequencies in scalp-level EEG recordings without proper shielding for environmental
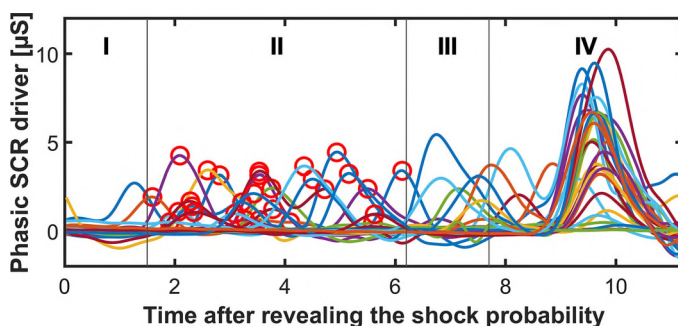
Figure 2. Phasic skin conductance response (SCR) driver for one participant after turning the first card (*t* = 0). SCR peaks within the time interval I were most likely not related to risk processing as they occurred too early. SCR peaks within time intervals II and III were considered to reflect risk-sensitive SCRs. For the analysis, only SCR peaks within period II were used (see red circles), because brain activity after SCR peaks in period III was most likely contaminated by processing of the second card. SCR peaks within time interval IV were due to turning of the second card and sometimes due to electric shock application and hence excluded from the analysis.

influences are often affected by artifacts (e.g., power line-noise at 50 Hz). Moreover, ongoing fluctuations in cortical activity are often found in lower frequencies, whereas the γ-band above 35 Hz is often associated with bottom-up stimulus processing (17). For each participant, single-segment data were projected into source space. To this end, a three-dimensional grid was calculated with a resolution of 15 mm covering the entire brain volume of the Montreal Neurological Institute standard brain (MNI; http://www.mni.mcgill.ca). To project raw data onto the grid points, they were multiplied with accordant spatial filters, thereby creating so-called virtual electrodes (39). This was done separately for each participant and grid point using a realistic three-shell boundary-element volume conduction model based on the MNI standard brain. Using a linear constrained minimum variance beamformer (40), a common filter was constructed across peak and dummy segments from the covariance matrix of the averaged single segments at sensor level and the respective leadfield. The filter was calculated for the entire 3-s segment ranging from −1.5 to 1.5 s around real SCR or dummy SCR peaks, respectively. The λ regularization parameter was set to 10%. The anatomical regions of the source localization were determined based on the automated anatomic labeling (AAL) atlas (41).

The third data analysis step consisted of the analysis of oscillatory power. To this end, the source-projected data segments at virtual electrodes were split into three consecutive 1-s intervals before (−1.5 to −0.5 s), around (−0.5 to 0.5 s), and after (0.5 to 1.5 s) real and dummy SCR peaks and transformed into the frequency domain using multitaper fast Fourier transformation (FFT; 42). The frequency band of 2–35 Hz was divided into steps of 1 Hz. Discrete prolate spheroidal sequence (DPSS) tapering was used with a spectral smoothing of ±2 Hz. The rationale for studying the above-mentioned 1-s time intervals (−1.5 to −0.5 s; −0.5 to 0.5 s; 0.5 to 1.5 s) was that Benedek and Kaernbach (26) show that SCR peaks occur around 2 ± 0.5 s after external events (noise bursts). Assuming that the time lag between an external event and the SCR peak should be larger than the time lag between an internal event and the SCR peak, we expected that the internal event responsible for the SCR peak should be captured within 1 ± 0.5 s before the SCR peak. To capture possible reafferent processes following the SCR peak, we applied the same window after the SCR peak. For completeness, we also studied the time interval around the SCR peak.

Statistical Analysis

To differentiate brain processes related to SCRs and general activity due to shock anticipation, we assessed differences in oscillatory power between real and dummy SCR peaks. To this end, we conducted a nonparametric cluster-based permutation test that addresses the multiple-comparison problem by clustering together samples adjacent in frequency and space (43). The experimental cluster-based test statistic was evaluated against a permutation distribution to test the null hypothesis of no difference between brain processes related to SCRs and general activity using a two-tailed dependent-samples test. The critical α-level was adjusted for three consecutive comparisons to 0.05/3 = 0.016. In short, this approach compares power for each frequency at each

virtual electrode. To control for multiple comparisons across the two-dimensional matrix of 463 (virtual electrodes) × 34 (frequencies) comparisons, the clustering algorithm searches for neighboring elements below the critical α-level and sums the t values in these clusters. Then the condition labels are shuffled, and the same comparison is computed on the shuffled data. This shuffling step is repeated for 5,000 iterations, and for each iteration, the largest sum of t values is retained ("maxsum" setting). Finally, the t value sums in the clusters of the empirical data are compared with the distribution of the clusters obtained in iterations. The P value for each empirical cluster, thus, is a percentile indicating the likelihood to obtain a cluster of this size based on randomly shuffled data. Importantly, the clusters obtained in this analysis are not due to any a priori selection of a frequency band but are solely based on the empirical data.

To illustrate the statistical results in more detail, we computed parametric dependent-samples t tests and Bayes factors (BF10; 44) as an indicator of the relative evidence for the H0 and H1 on the power averaged within the clusters identified in the previous steps. BFs between 1 and 3 indicate anecdotal support for the alternative hypothesis (H1), whereas BFs between 3 and 10 and above 10 indicate, respectively, moderate and strong support for H1. BF = 1 indicates equal support for H1 and null hypothesis (H0), whereas BFs between 1/3 and 1, 1/10 and 1/3, and below 1/10 provide, respectively, anecdotal, moderate, and strong support for H0 (45). Finally, we related single-segment oscillatory power based on the result of the comparison between real and dummy SCR peaks to the SCR peak amplitude. To this end, we used a random-intercept model (package lme4 in R) to account for the dependencies among repeated data.

Analysis scripts and stimulus material are available at https://doi.org/10.17605/OSF.IO/BWSE4.

RESULTS

Influence of Shock Probability on SCR Measures

We verified that our experimental task was successful in eliciting risk-sensitive SCRs, as suggested by the previous literature with this particular design (27, 29, 30). To account for the dependencies among repeated data, we used random intercept models (package lme4 in R), which allow each participant to have a unique intercept (32). The models showed that the shock probability had a positive and statistically significant impact on various SCR measures (integrated SCR: β = 2.965, SE = 0.317, $P < 0.001$; sum of SCR amplitude: β = 0.783, SE = 0.081, $P < 0.001$; number of SCR peaks: β = 1.011, SE = 0.135, $P < 0.001$; see Table 1). The averaged integrated SCRs for the different shock probabilities can be found in Fig. 3. We can, therefore, conclude that our experimental design was successful in eliciting risk-sensitive SCRs. The distribution of SCR peaks across the different shock probability levels is reported in Table 2. Please note that the generated dummy SCR peaks had the exact same distributional characteristics as the real SCR peaks.

Oscillatory Power

Surface-level EEG data were projected onto 463 virtual electrodes in source space. We tested for a difference in

Table 1. *Regression analyses of various SCR measures on shock probability*

	Dependent Variable		
	Integrated SCR (1)	Sum of SCR Amplitudes (2)	Number of SCR Peaks (3)
Shock probability	2.965*** (0.317)	0.783*** (0.081)	1.011*** (0.135)
Constant	0.559** (0.200)	0.108* (0.055)	0.558*** (0.099)
Observations	1,500	1,500	1,500
Groups	25	25	25

Standard errors are given in parentheses. SCR, skin conductance response. *$P < 0.05$; **$P < 0.01$; ***$P < 0.001$.

oscillatory power (2–35 Hz) in the three intervals (−1.5 to −0.5 s, −0.5 to 0.5 s, and 0.5 to 1.5 s) around the identified SCR peaks and the dummy SCR peaks assigned artificially. The cluster-based permutation test revealed a significant difference in power between the real and dummy SCR peaks in the first interval (cluster-P = 0.0072) but not in the other two intervals. The difference visible in the first interval was most pronounced in occipitotemporal cortical areas, in the frequency range of 3–17 Hz. Comparison with the AAL atlas indicated the left lingual gyrus as the source of the peak difference. The power averaged over the significant channel-by-frequency cluster before the SCR peaks (means ± SD: $0.7154 \times 10^7 \pm 0.3760 \times 10^7$) was lower than before the dummy SCR peaks (means ± SD: $0.7821 \times 10^7 \pm 0.4447 \times 10^7$) [$t(18) = -2.5699$, P = 0.0193, CI = (-0.1210×10^7 to 0.0121×10^7), BF10 = 2.27, see Fig. 4]. For exploratory purposes, we examined the time course of the α-power in the identified source space cluster. In this post hoc analysis, we found that the α-power was reduced for real compared with dummy SCR peaks from around −1.6 to −0.4 s before peak onset, indicating the robustness of our results with respect to exact time windows.

To estimate the relationship between the single-segment oscillatory power and the SCR peak amplitude, we averaged the power across the cluster identified in comparison between real and dummy SCR peaks within each segment and participant. Then, we used a random-intercept model (package lme4 in R) to account for the dependencies among repeated data. The model showed that the oscillatory power averaged across 3–17 Hz had a small but statistically significant negative impact on the SCR peak amplitude (β = −0.464, SE = 0.131, $P < 0.001$), indicating that reduced power was associated with increased SCR peak amplitudes.

DISCUSSION

Understanding the neural correlates of risk-sensitive skin conductance responses can provide insights into their connection to emotional and cognitive processes. Therefore, we studied oscillatory brain activity based on event-related analyses of asynchronously distributed SCR peaks to identify cortical processes associated with risk-sensitive SCRs and their possible reafferent representation. In contrast to previous studies, we applied methods with high-temporal resolution, that is, EEG analysis for brain activity and a temporally precise decomposition method for electrodermal activity. We, thus, took advantage of the temporally precise nature of sympathetic activity (24, 25). Fluctuations in SCRs were elicited while participants played a threat-of-shock card game. To exclude brain activity related to electric shock anticipation, we generated dummy SCR peaks, which had identical distributional characteristics as real SCR peaks but no temporal connection to real SCR peaks. Brain activity related to dummy SCR peaks was compared with activity related to real SCR peaks. Within the time interval of −1.5 to −0.5 s preceding real SCR peaks, we observed reduced oscillatory power in the frequency range between 3 and 17 Hz in occipitotemporal cortical areas. Comparison with the AAL atlas indicated the left lingual gyrus as the source of the power difference. However, labeling of deep cortical generators is not exact due to the low-spatial resolution of EEG data. In intervals following SCR peaks, we did not find systematic differences between real and dummy SCR peaks. Reduced single-segment occipitotemporal oscillatory power was related to increased SCR peak amplitudes.
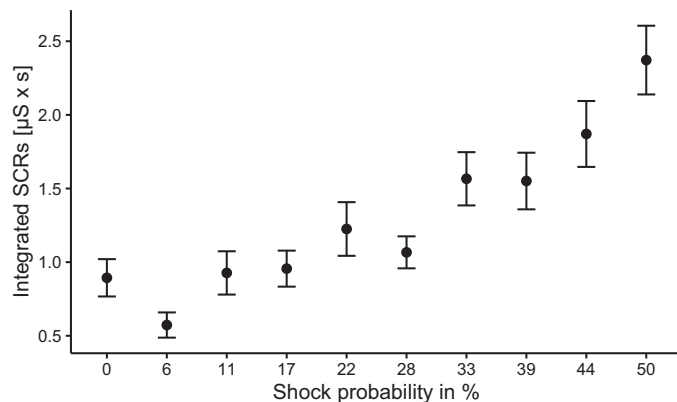
Figure 3. Averaged integrated skin conductance responses (SCRs) by shock probability. Error bars indicate the standard errors of the mean.

Table 2. *Distributional characteristics of SCR peaks depending on the shock probability*

Shock Probability, %	Share of Total SCR Peaks, %
0	8.6
6	6.6
11	8.6
17	9
22	9
28	9.6
33	10.6
39	11
44	12
50	15

SCR, skin conductance response.

Oscillatory brain activity, particularly in the α-band (8–12 Hz), has been implicated in regulating selective attention (20, 46, 47). More precisely, it has been argued that α-activity is important for attentional inhibition. Increased α-band power has been linked to suppressing information that is irrelevant and potentially distracting. In turn, reduced α-band power is related to the processing of relevant information: reduced α-power allows to sequentially process bits of information and prioritize the resulting objects according to salience, which can then capture attention based on subjective relevance (20). A study on social decisions found that α-band power was reduced before feedback in high-risk situations, suggesting a sensitivity to risk perception (23). In our experiment, before an electric shock, we observed reduced power in the frequency range between 3 and 17 Hz, which comprises the θ (4–7 Hz), α (8–12 Hz), and β (13–30 Hz) ranges, but appears to be maximal for the α-band (Fig. 4A). However, the reduced power was not due to the anticipation of the shock itself. Since real and dummy SCR peaks were perfectly matched in terms of shock probabilities, the reduced power before threat-related SCRs in visual processing areas might be an expression of attention, that is, the processing of task-relevant information in threat situations. A related finding has been reported by Lim et al. (48) who observed a significant negative correlation between the logarithm of the SCR amplitude and EEG-α activity in an auditory oddball task without threat processing. Similarly, we found a small but significant negative correlation between
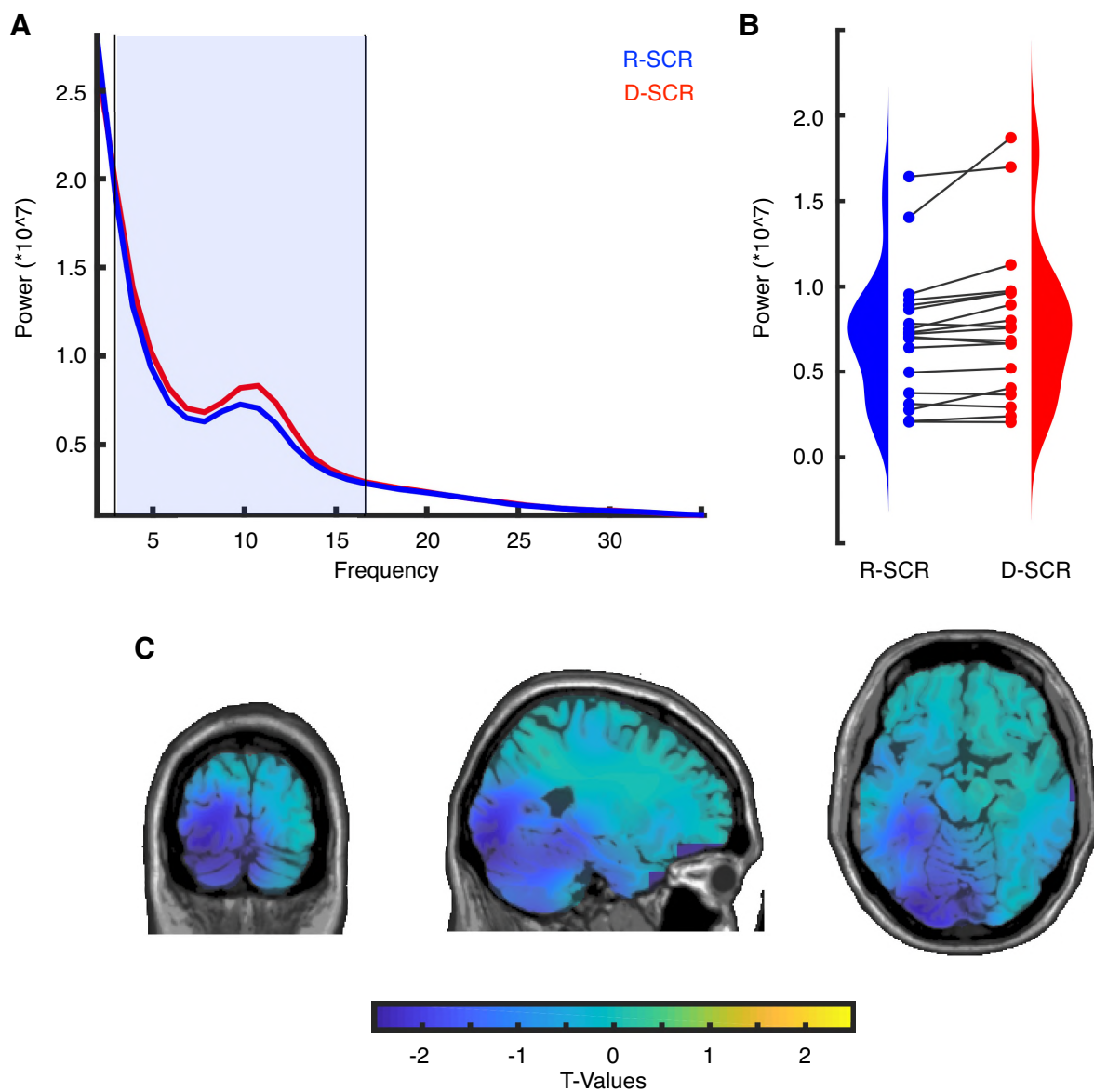
Figure 4. Results of the analysis of oscillatory power in the first interval. *A*: averaged power spectrum for the cluster identified in the comparison between real (R-SCR) and dummy (D-SCR) SCR peak segments. The box highlights the frequency range (3–17 Hz) in which a significant difference was found. *B*: oscillatory power averaged over the frequency range highlighted in *A* for real (R-SCR) and dummy (D-SCR) SCR peak segments. *C*: spatial extent of the cluster identified in the comparison between real and dummy SCR peak segments for the frequency range highlighted in *A*. Colors represent *t* values. SCR, skin conductance response.

the occipitotemporal α-band amplitude and the SCR peak amplitude.

In addition to attention, arousal appears to lead to reduced α-band power. For example, resting-state α-band power has been reported to be correlated negatively with arousal (21), and stimulus-induced α-band power reduction possible reflects emotional arousal (22). Thus, our findings of reduced α-band power before SCRs may indicate intensified attentional and emotional processing of task-relevant information in threat situations. Two alternative hypotheses could explain this finding. On the one hand, it is conceivable that α-power signals fluctuating attention during threat situations. If attention is high, the threat perception will elicit sympathetic response. This hypothesis is also supported by the delay of the SCR peak after the α-power reduction. Since electrodermal activity is transmitted via slow, unmyelinated fibers (49), SCR peaks will occur with a delay after attention pushes the threat signal across a threshold. On the other hand, it is conceivable that a common process influences cortical α and sympathetic responses. If a threat is perceived, this bottom-up information could capture attention and lead to an SCR peak. Because the sympathetic response is transmitted slower than the cortical activation, the α-power decrease will precede the SCR peak. To differentiate between these two hypotheses, future research is needed to examine the temporal profile of α-power changes in more detail and to study the underlying functional connectivity networks. One starting point could be using invasive electrophysiological recording (electrocorticography) directly from the occipital cortex while simultaneously recoding SCRs to track the temporal dynamics.

The largest difference in observed SCR-related oscillatory power in visual-processing areas was localized in the lingual gyrus. The lingual gyrus has been implicated in the processing of complex visual stimuli (50). Moreover, functional MRI (fMRI) and EEG studies reported increased activation during working memory tasks and emotional processing (51, 52). Activity in visual areas, especially the lingual gyrus, preceding discrete SCRs has also been reported in an fMRI study by Critchley et al. (12), indicating converging findings across modalities. This finding was interpreted to represent modulation of areas involved in processing the visual stimuli that carry information about reinforcement by arousal. Varying activity in higher-order visual processing areas may be due to processing of the visual stimulus (in our case the card value) reflecting its fluctuating salience. Thus, the reduced α-band power in lingual gyrus could be a sign that SCRs indicate the increased processing of the cards' information in the context of the task setting as well as the emotional processing of the threat probability. It would be interesting to see if in a study without ongoing visual stimulus, similar brain areas are part of the network. Moreover, it is known that SCR peaks occur delayed after the onset of an external event (26, 53). In the current experiment, no such external events were presented, but SCR peaks were examined during the anticipation of an electric shock. Therefore, it would be interesting to examine the cortical generators of SCR peaks with a known eliciting event such as noise bursts.

We did not observe activity in the VMPFC, which has been identified by Bechara and Damasio (54) as an important brain area related to SCRs, and we did not find any differences after SCR peaks that would have indicated reafference processing. As outlined above, the neural correlates of SCRs depend on the type of stimulus and on the SCR function. Patients with lesions of the amygdala or VMPFC, for example, fail to produce anticipatory SCRs to motivationally relevant stimuli but not physical stimuli. Furthermore, Damasio and colleagues (1, 55) stress the role of the VMPFC in storing implicit knowledge about the anticipated value of a choice. In our experiment, however, shock probabilities were explicitly stated and did not depend on participants' decisions. Therefore, associations between the VMPFC and bodily responses might have been less important in our context. Another perspective on this might be given by Tomb et al. (56), suggesting that VMPFC activity signals not the valence but the variance (risk) of payoffs driving SCR responses in the IGT. Since in our study, real and dummy SCR peaks were perfectly matched in terms of risk, VMPFC signaling might be canceled out. All in all, it is left for future research to carefully identify different "types" of SCRs, their exact functioning, and their neuroanatomical basis.

In conclusion, this study characterized the cortical correlates of risk-sensitive SCRs. Our results suggest an interaction between attention and emotion such as threat perception reflected in skin conductance responses.

DISCLOSURES

No conflicts of interest, financial or otherwise, are declared by the authors.

AUTHOR CONTRIBUTIONS

P.R., S.W., C.P., L.N., U.S., T.v.E., and C.K. conceived and designed research; P.R., M.M., S.W., C.P., and L.N. performed experiments; P.R. and J.K. analyzed data; P.R., J.K., M.M., T.O.B., U.S., T.v.E., and C.K. interpreted results of experiments; P.R. and J.K. prepared figures; P.R., J.K., and C.K. drafted manuscript; P.R., J.K., M.M., S.W., T.O.B., C.P., L.N., U.S., T.v.E., and C.K. edited and revised manuscript; P.R., J.K., M.M., S.W., T.O.B., C.P., L.N., U.S., T.v.E., and C.K. approved final version of manuscript.

ENDNOTE

At the request of the authors, readers are herein alerted to the fact that additional materials related to this manuscript may be found at https://doi.org/10.17605/OSF.IO/BWSE4. These materials are not a part of this manuscript and have not undergone peer review by the American Physiological Society (APS). APS and the journal editors take no responsibility for these materials, for the website address, or for any links to or from it.

REFERENCES

1. **Bechara A**, **Damasio H**, **Tranel D**, **Damasio AR.** Deciding advantageously before knowing the advantageous strategy. *Science* 275: 1293–1295, 1997. doi:10.1126/science.275.5304.1293.
2. **Valins S.** Cognitive effects of false heart-rate feedback. *J Pers Soc Psychol* 4: 400–408, 1966. doi:10.1037/h0023791.
3. **Gu J**, **Zhong CB**, **Page-Gould E.** Listen to your heart: when false somatic feedback shapes moral behavior. *J Exp Psychol Gen* 142: 307–312, 2013. doi:10.1037/a0029549.
4. **Boucsein W.** *Electrodermal Activity* (2nd ed.). New York: Springer Science + Business Media, 2012. doi:10.1007/978-1-4614-1126-0.
5. **Ojala KE**, **Bach DR.** Measuring learning in human classical threat conditioning: translational, cognitive and methodological considerations. *Neurosci Biobehav Rev* 114: 96–112, 2020. doi:10.1016/j.neubiorev.2020.04.019.
6. **Critchley HD.** Electrodermal responses: what happens in the brain. *Neuroscientist* 8: 132–142, 2002. doi:10.1177/107385840200800209.
7. **Bechara A**, **Damasio H**, **Damasio AR**, **Lee GP.** Different contributions of the human amygdala and ventromedial prefrontal cortex to decision-making. *J Neurosci* 19: 5473–5481, 1999. doi:10.1523/jneurosci.19-13-05473.1999.
8. **Bechara A**, **Tranel D**, **Damasio H**, **Adolphs R**, **Rockland C**, **Damasio AR.** Double dissociation of conditioning and declarative knowledge relative to the amygdala and hippocampus in humans. *Science* 269: 1115–1118, 1995. doi:10.1126/science.7652558.
9. **Tranel D**, **Damasio H.** Neuroanatomical correlates of electrodermal skin conductance responses. *Psychophysiology* 31: 427–438, 1994. doi:10.1111/j.1469-8986.1994.tb01046.x.
10. **Mangina CA**, **Beuzeron-Mangina JH.** Direct electrical stimulation of specific human brain structures and bilateral electrodermal activity. *Int J Psychophysiol* 22: 1–8, 1996. doi:10.1016/0167-8760(96)00022-0.
11. **Sequeira H**, **Ba-M'Hamed S**, **Roy JC.** Fronto-parietal control of electrodermal activity in the cat. *J Auton Nerv Syst* 53: 103–114, 1995. doi:10.1016/0165-1838(94)00177-L.
12. **Critchley HD**, **Elliott R**, **Mathias CJ**, **Dolan RJ.** Neural activity relating to generation and representation of galvanic skin conductance responses: a functional magnetic resonance imaging study. *J Neurosci* 20: 3033–3040, 2000. doi:10.1523/jneurosci.20-08-03033.2000.
13. **Fan J**, **Xu P**, **Van Dam NT**, **Eilam-Stock T**, **Gu X**, **Luo Y-J**, **Hof PR.** Spontaneous brain activity relates to autonomic arousal. *J Neurosci* 32: 11176–11186, 2012. doi:10.1523/JNEUROSCI.1172-12.2012.
14. **Fredrikson M**, **Furmark T**, **Olsson MT**, **Fischer H**, **Andersson J**, **Långström B.** Functional neuroanatomical correlates of electrodermal activity: a positron emission tomographic study. *Psychophysiology* 35: 179–185, 1998. doi:10.1111/1469-8986.3520179.
15. **Gertler J**, **Novotny S**, **Poppe A**, **Chung YS**, **Gross JJ**, **Pearlson G**, **Stevens MC.** Neural correlates of non-specific skin conductance responses during resting state fMRI. *NeuroImage* 214: 116721, 2020. doi:10.1016/j.neuroimage.2020.116721.
16. **Patterson JC 2nd**, **Ungerleider LG**, **Bandettini PA.** Task-independent functional brain activity correlation with skin conductance changes: an fMRI study. *NeuroImage* 17: 1797–1806, 2002. doi:10.1006/nimg.2002.1306.
17. **Cohen MX.** Where does EEG come from and what does it mean? *Trends Neurosci* 40: 208–218, 2017. doi:10.1016/j.tins.2017.02.004.
18. **Buzsáki G**, **Draguhn A.** Neuronal oscillations in cortical networks. *Science* 304: 1926–1929, 2004. doi:10.1126/science.1099745.
19. **Siegel M**, **Engel AK**, **Donner TH.** Cortical network dynamics of perceptual decision-making in the human brain. *Front Hum Neurosci* 5: 21, 2011. doi:10.3389/fnhum.2011.00021.
20. **Jensen O**, **Bonnefond M**, **VanRullen R.** An oscillatory mechanism for prioritizing salient unattended stimuli. *Trends Cogn Sci* 16: 200–206, 2012. doi:10.1016/j.tics.2012.03.002.
21. **Barry RJ**, **De Blasio FM**, **Fogarty JS**, **Clarke AR.** Natural alpha frequency components in resting EEG and their relation to arousal. *Clin Neurophysiol* 131: 205–212, 2020. doi:10.1016/j.clinph.2019.10.018.
22. **Schubring D**, **Schupp HT.** Affective picture processing: alpha- and lower beta-band desynchronization reflects emotional arousal. *Psychophysiology* 56: e13386, 2019. doi:10.1111/psyp.13386.
23. **Billeke P**, **Zamorano F**, **Cosmelli D**, **Aboitiz F.** Oscillatory brain activity correlates with risk perception and predicts social decisions. *Cereb Cortex* 23: 2872–2883, 2013. doi:10.1093/cercor/bhs269.
24. **Macefield VG**, **Wallin BG.** The discharge behaviour of single sympathetic neurones supplying human sweat glands. *J Auton Nerv Syst* 61: 277–286, 1996. doi:10.1016/S0165-1838(96)00095-1.
25. **Mano T**, **Iwase S**, **Toma S.** Microneurography as a tool in clinical neurophysiology to investigate peripheral neural traffic in humans. *Clin Neurophysiol* 117: 2357–2384, 2006. doi:10.1016/j.clinph.2006.06.002.
26. **Benedek M**, **Kaernbach C.** A continuous measure of phasic electrodermal activity. *J Neurosci Methods* 190: 80–91, 2010. doi:10.1016/j.jneumeth.2010.04.028.
27. **Ring P**, **Kaernbach C.** Sensitivity towards fear of electric shock in passive threat situations. *PLoS One* 10: e0120989, 2015. doi:10.1371/journal.pone.0120989.
28. **Preuschoff K**, **Quartz SR**, **Bossaerts P.** Human insula activation reflects risk prediction errors as well as risk. *J Neurosci* 28: 2745–2752, 2008. doi:10.1523/JNEUROSCI.4286-07.2008.
29. **Ring P**, **Probst CC**, **Neyse L**, **Wolff S**, **Kaernbach C**, **van Eimeren T**, **Camerer CF**, **Schmidt U.** It's all about gains: risk preferences in problem gambling. *J Exp Psychol Gen* 147: 1241–1255, 2018. doi:10.1037/xge0000418.
30. **Ring P.** The framing effect and skin conductance responses. *Front Behav Neurosci* 9: 188, 2015. doi:10.3389/fnbeh.2015.00188.
32. **Bagiella E**, **Sloan RP**, **Heitjan DF.** Mixed-effects models in psychophysiology. *Psychophysiology* 37: 13–20, 2000. doi:10.1017/S0048577200980648.
33. **Oostenveld R**, **Fries P**, **Maris E**, **Schoffelen JM.** FieldTrip: Open source software for advanced analysis of MEG, EEG, and invasive electrophysiological data. *Comput Intell Neurosci* 2011: 156869, 2011. doi:10.1155/2011/156869.
34. **Delorme A**, **Makeig S.** EEGLAB: an open source toolbox for analysis of single-trial EEG dynamics including independent component analysis. *J Neurosci Methods* 134: 9–21, 2004. doi:10.1016/j.jneumeth.2003.10.009.
35. **Widmann A**, **Schröger E**, **Maess B.** Digital filter design for electrophysiological data — a practical approach. *J Neurosci Methods* 250: 34–46, 2015. doi:10.1016/j.jneumeth.2014.08.002.
36. **Bigdely-Shamlo N**, **Mullen T**, **Kothe C**, **Su KM**, **Robbins KA.** The PREP pipeline: standardized preprocessing for large-scale EEG analysis. *Front Neuroinform* 9: 16, 2015. doi:10.3389/fninf.2015.00016.
37. **Lee TW**, **Girolami M**, **Sejnowski TJ.** Independent component analysis using an extended infomax algorithm for mixed subgaussian and supergaussian sources. *Neural Comput* 11: 417–441, 1999. doi:10.1162/089976699300016719.
38. **Chaumon M**, **Bishop DVM**, **Busch NA.** A practical guide to the selection of independent components of the electroencephalogram for artifact correction. *J Neurosci Methods* 250: 47–63, 2015. doi:10.1016/j.jneumeth.2015.02.025.
39. **Keil A**, **Debener S**, **Gratton G**, **Junghöfer M**, **Kappenman ES**, **Luck SJ**, **Luu P**, **Miller GA**, **Yee CM.** Committee report: publication guidelines and recommendations for studies using electroencephalography and magnetoencephalography. *Psychophysiology* 51: 1–21, 2014. doi:10.1111/psyp.12147.
40. **Van Veen BD**, **Van Drongelen W**, **Yuchtman M**, **Suzuki A.** Localization of brain electrical activity via linearly constrained minimum variance spatial filtering. *IEEE Trans Biomed Eng* 44: 867–880, 1997. doi:10.1109/10.623056.
41. **Tzourio-Mazoyer N**, **Landeau B**, **Papathanassiou D**, **Crivello F**, **Etard O**, **Delcroix N**, **Mazoyer B**, **Joliot M.** Automated anatomical labeling of activations in SPM using a macroscopic anatomical parcellation of the MNI MRI single-subject brain. *NeuroImage* 15: 273–289, 2002. doi:10.1006/nimg.2001.0978.
42. **Percival DB**, **Walden AT.** *Wavelet Methods for Time Series Analysis*. New York: Cambridge University Press, 2000. doi:10.1017/CBO9780511841040.
43. **Maris E**, **Oostenveld R.** Nonparametric statistical testing of EEG- and MEG-data. *J Neurosci Methods* 164: 177–190, 2007. doi:10.1016/j.jneumeth.2007.03.024.
44. **Rouder JN**, **Speckman PL**, **Sun D**, **Morey RD**, **Iverson G.** Bayesian *t* tests for accepting and rejecting the null hypothesis. *Psychon Bull Rev* 16: 225–237, 2009. doi:10.3758/PBR.16.2.225.
45. **Aczel B**, **Palfi B**, **Szaszi B.** Estimating the evidential value of significant results in psychological science. *PLoS One* 12: e0182651, 2017. doi:10.1371/journal.pone.0182651.

46. **Klimesch W.** Alpha-band oscillations, attention, and controlled access to stored information. *Trends Cogn Sci* 16: 606–617, 2012. doi:10.1016/j.tics.2012.10.007.

47. **Mathewson KE, Lleras A, Beck DM, Fabiani M, Ro T, Gratton G.** Pulsed out of awareness: EEG alpha oscillations represent a pulsed-inhibition of ongoing cortical processing. *Front Psychol* 2: 99, 2011. doi:10.3389/fpsyg.2011.00099.

48. **Lim CL, Rennie C, Barry RJ, Bahramali H, Lazzaro I, Manor B, Gordon E.** Decomposing skin conductance into tonic and phasic components. *Int J Psychophysiol* 25: 97–109, 1997. doi:10.1016/S0167-8760(96)00713-1.

49. **Kennedy WR, Wendelschafer-Crabb G, Brelje TC.** Innervation and vasculature of human sweat glands: an immunohistochemistry-laser scanning confocal fluorescence microscopy study. *J Neurosci* 14: 6825–6833, 1994. doi:10.1523/jneurosci.14-11-06825.1994.

50. **Cabeza R, Nyberg L.** Imaging cognition II: an empirical review of 275 PET and fMRI studies. *J Cogn Neurosci* 12: 1–47, 2000. doi:10.1162/08989290051137585.

51. **Keil A, Costa V, Smith JC, Sabatinelli D, McGinnis EM, Bradley MM, Lang PJ.** Tagging cortical networks in emotion: a topographical analysis. *Hum Brain Mapp* 33: 2920–2931, 2012. doi:10.1002/hbm.21413.

52. **Sabb FW, Bilder RM, Chou M, Bookheimer SY.** Working memory effects on semantic processing: priming differences in pars orbitalis. *NeuroImage* 37: 311–322, 2007. doi:10.1016/j.neuroimage.2007.04.050.

53. **Bach DR, Flandin G, Friston KJ, Dolan RJ.** Modelling event-related skin conductance responses. *Int J Psychophysiol* 75: 349–356, 2010. doi:10.1016/j.ijpsycho.2010.01.005.

54. **Bechara A, Damasio AR.** The somatic marker hypothesis: a neural theory of economic decision. *Games Econ Behav* 52: 336–372, 2005. doi:10.1016/j.geb.2004.06.010.

55. **Damasio AR.** *Descartes Error: Emotion, Reason and the Human Brain*. New York: Putnam, 1994.

56. **Tomb I, Hauser M, Deldin P, Caramazza A.** Do somatic markers mediate decisions on the gambling task? *Nat Neurosci* 5: 1103–1104, 2002. doi:10.1038/nn1102-1103.